ELSEVIER

International Journal of Heat and Fluid Flow 22 (2001) 350–357

International Journal of HEAT AND FLUID FLOW

www.elsevier.com/locate/ijhff

Fuel deposition and re-atomisation from fuel/air flows through engine inlet valves

B.E. Milton *, M. Behnia, D.M. Ellerman

School of Mechanical and Manufacturing Engineering, University of NSW, M.E. Building, Room M33, Sydney, NSW 2052, Australia

Abstract

The two-phase fuel/air flow through an internal combustion engine inlet valve has been studied experimentally in a specially designed rig. The separated flow associated with fuel films on the inlet port and large droplets on the valve stem can be readily seen. Injector location, valve lift and air stream velocity all influence the subsequent re-entrainment and secondary atomisation of the fuel. Deposition into discrete regions below the valve occurs. Numerical simulation of the airflow shows good agreement with the experiments. © 2001 Elsevier Science Inc. All rights reserved.

Keywords: Gasoline engine induction flows; Fuel/air flows; Inlet valve flows

1. Introduction

The mixing of the fuel and air in spark ignition engines is a critical factor in obtaining good performance together with low emission levels. While the overall air/fuel ratio may readily be held at the optimum value at the injection point, many time-dependent excursions occur within the cylinders due to the differences in the transport velocities of the fuel from the injection point. That is, the air and vapor mixture, the liquid droplets and the fuel streams deposited on the walls have significantly different velocities. The last of these provides the most significant factor that is particularly noticeable during operational transients, which include acceleration, deceleration and warm-up periods. While it has long been evident that throttle body (single point systems) are likely to have poor response to such changes as noted by Collins (1969) and Tanaka and Durbin (1977), more recent work by, for example, Shayler et al. (1993) indicates that port (multi-point) injection experiences similar problems. Poor response during cold start is still noticeable. Even in a fully warmed-up engine with higher evaporated fuel proportions, considerable fuel in the liquid phase still enters the engine and lag problems occur during transients. As well as temporal imbalances, recent research (Saito et al., 1995; Takeda et al., 1995; Shin et al., 1995), has shown that spatial fuel maldistribution can occur within the cylinders. This is because droplets and films within the port may, with some re-atomization, pass through open inlet valves and re-deposit on the piston crown and cylinder walls. Fig. 1 depicts such a situation. Fry et al. (1995) found significant wall wetting of the inlet port in a pent-roof port injected engine with film formation within the combustion chamber adjacent to the valves and on the piston crown by use of high-speed cine cameras. Some combustion chamber film survived combustion to be subsequently drawn into the exhaust.

2. Fuel films measurements in engine inlet manifolds and ports

2.1. Previous studies

The flows are two-phase, separated, multi-component (with different evaporation rates), unsteady and turbulent (Milton and Behnia, 1988). Hence, they are highly complex. In engines, the formation, movement, stripping, re-atomisation and evaporation of fuel films are some of the most important aspects of the flow but the hardest to study. To improve understanding of such flows, specific experimental rigs with associated numerical simulation of the flow details are beneficial. These can provide the appropriate viewing and measurement sections so that the flow can be studied in detail. This latter approach has been followed in the present research.

Film flow can be measured either indirectly by estimating the airborne droplet and vapour quantities or directly. The former approach ranges from the use of a traversing suction probe to draw off airborne fuel vapour and liquid (Collins, 1969) to infrared techniques (Wagner and Nemecek, 1997). The direct approach has included the use of conductive probes (Hayashi and Sawa, 1984) to measure film thickness, trapping to obtain film flow rate (Hasson and Flint, 1989) and hot wire probes to determine the film velocity (Hohsho et al., 1985).

* Corresponding author. Tel.: +61-2-9385-5699; fax: +61-2-9663-1222.

E-mail address: b.milton@unsw.edu.au (B.E. Milton).

PII: S0142-727X(01)00098-4

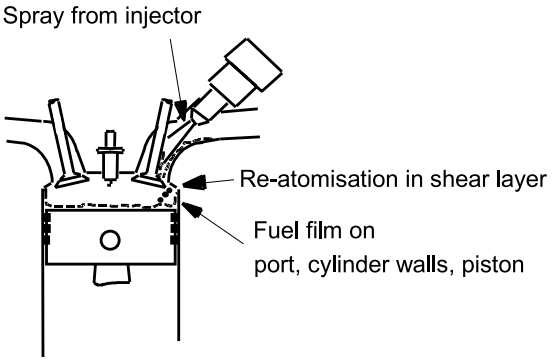

Fig. 1. Fuel injection in an inlet port.

2.2. The current programme

2.2.1. Experiments

Special rigs were developed for the present project as depicted in Fig. 2. Fuel film velocities and depths and have been measured (Milton et al., 1997; Behnia and Milton, 1998) for a range of steady, unsteady and turbocharged conditions around butterfly valves, in straight, horizontal manifolds and at manifold bends. Fuel film velocities are consistently two orders of magnitude less than the average gas stream velocity.

2.2.2. Numerical simulation

The numerical simulation uses several codes. These are:

1. a purpose developed in-house one-dimensional simulation code (Milton and Behnia, 1988);
2. a multi-dimensional numerical examination of the base air flows in complex regions (e.g., the butterfly valve wake) using general purpose, proprietary CFD codes;
3. an in-house Monte Carlo technique, coupled with the output of (2), that is based on experimental distributions of droplets in sprays (Milton et al., 1994).

3. Two-phase flow through inlet valves

The air and fuel flow through the inlet valve is of major importance particularly in port injection systems as much of the fuel is deposited from the injector onto the port wall or the back of the inlet valve. Hence, the transmission, stripping and secondary atomisation of the film by the airflow as it passes through an inlet valve is now being studied. At present, all tests are being carried out on the rig using steady flow at naturally aspirated conditions with the inlet valve being set at a series of fixed positions consistent with the range of a normal engine. Experiments and numerical simulation are being undertaken. The basic configurations for the simulation and experiment are shown in Fig. 3.

3.1. Experiments

The separated fuel/air flows have been visualised using direct back-lit photography (Milton and Archer, 1998). Regions where the fuel is deposited into films can be identified for study, as can regions of dense airborne droplet flow. Previous studies in this programme have examined injection upstream of the throttle valve and at 90° bends. In the present study, the air flows around a 90° bend (port), through an engine inlet valve to a fixed volume, rectangular chamber (to simulate an engine cylinder). The fuel is injected in the port just upstream of the inlet valve. The valve is circular while the duct, port and chamber sections are rectangular for improved flow visualization.

3.1.1. Fuel injector location

Two injector locations were examined, the undisturbed centreline of the fuel either impinging on the port wall upstream of the inlet valve (block 1) or striking the lower part of the inlet valve stem (block 2). The valve used had a stem diameter of 5 mm and valve head outer diameter of 25 mm. The vertical walls are designated respectively as the near and far wall in relation to the manifold. The injection was oriented at 45° to the manifold airstream. For no flow, the exact location of the spray centreline at the lower wall is 24 mm and 8 mm

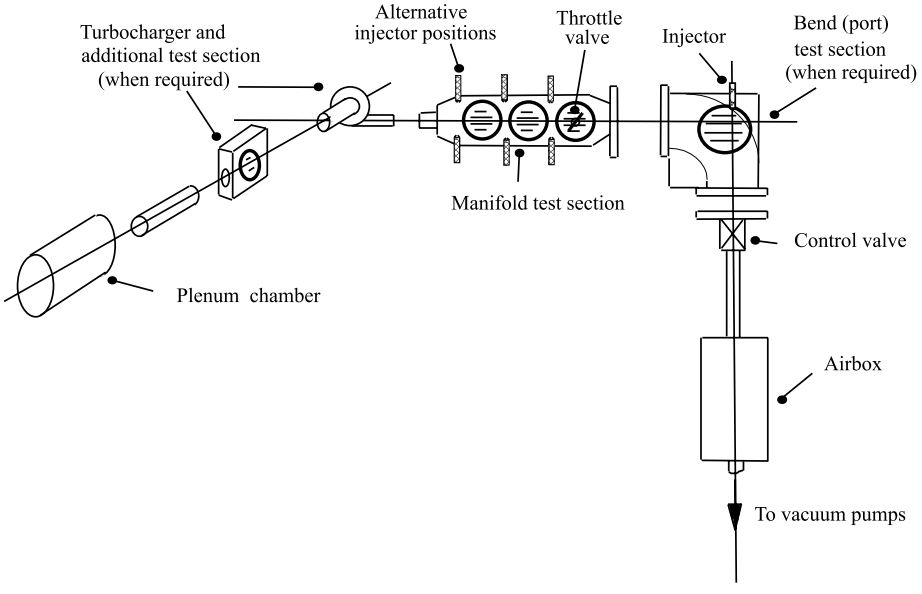

Fig. 2. Basic arrangement and sections of the rig.

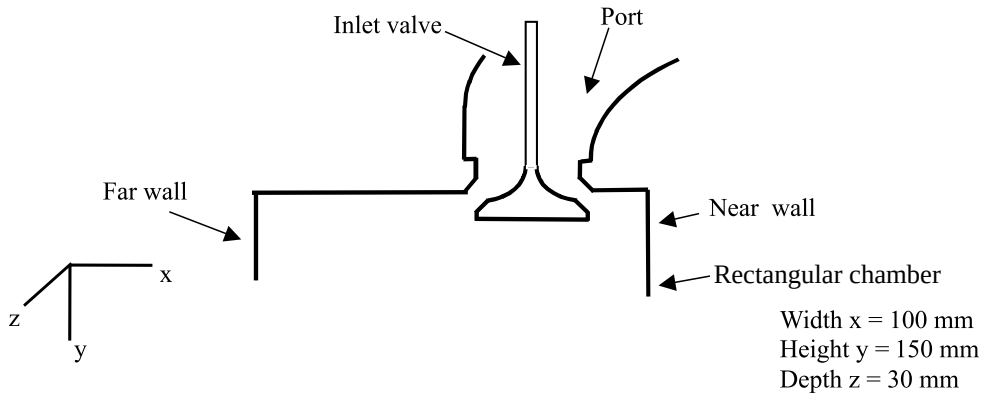

Fig. 3. Schematic of current test section.

upstream of the valve but this is modified by the air spray. Average airstream velocities in the manifold fall in the range 7.5–10.2 m/s with lowest inlet valve lift of 1 mm to 12–19 m/s at the maximum lift of 4 mm. In all cases, a stoichiometric fuel/air ratio was used.

Fig. 4 shows a typical view of the complete spray from injector to impact for a high valve lift, high airspeed condition. The deviation of the jet due to the influence of the airstream velocity is apparent. A substantial rebound of fuel droplets (Fig. 5) occurs from the lower wall, some impinging on the leading edge of the valve stem, some forming on the rear of the valve. A thick fuel film remains on the lower wall upstream of the valve.

Comparison of the flow for the two injector locations is given in Fig. 6. For block 1 (Fig. 6(a)), the fuel flow past the valve is heavily biased to the near-side with a heavy flow into the chamber originating from the lower wall film augmented by drainage from the valve stem. For block 2 (Fig. 6(b)), the film is distributed around the valve, the fuel flow through the valve being more uniform. The spray core now clearly intersects the valve stem forming many droplets on its surface with a substantial film flowing down the valve.

3.1.2. Effect of valve lift on flow downstream of valve

The flow on the downstream side of the valve is depicted in Figs. 7 and 8. Fig. 7 shows the effect of different valve lifts ranging from nearly closed (1 mm lift) to high (4 mm lift). The variation in velocity (see figure captions) is due to the different inlet valve restrictions.

For the 1 mm valve lift, the fuel from the film collects above the valve and is stripped and atomised by the high velocity gas flow through it. Average through-valve velocity, $V_{\text{valve air}}$, is estimated to be about 120 m/s. Much of the fuel is re-deposited downstream. As the valve lift is increased, a greater fuel flow below the valve to the near side can be seen. Also the droplet sizes downstream are coarser. This is because of the lower velocity through the valve that is now about 80 m/s. Fuel collects on the upper wall inside the chamber, particularly on the near wall corner from where it then drains down the near wall. The 4 mm valve lift has a through-flow velocity of 53 m/s. Again, substantial fuel quantities can be seen emanating from the valve to the near wall. The jet, aligned approximately along the valve surface, occurs in all directions and deposits onto the side wall. It now contains large droplets because the port film is not as well re-atomised as it passes through the inlet valve due to the lower valve airstream velocity.

With the low flow velocity and finely atomised drops as in the 1 mm valve lift case, the near wall flow is directed downwards within a few millimetres of the valve (Fig. 8(a)), not much fuel having accumulated in the upper wall film. It then collects in the clockwise vortex about two valve diameters D_V, below the valve forming a new film on the side wall with further droplet re-distribution from it back to the main gas-phase field, particularly towards the far wall. For the larger valve openings, an inverted U-shaped region forms directly below the valve to the bottom of the test section containing little fuel. The effect of this can be seen on the two glass walls. A high velocity jet down the near wall carrying very small droplets or vapour is apparent, with a wider efflux existing on the far side of the valve. Further on the far side, fuel can be seen streaming

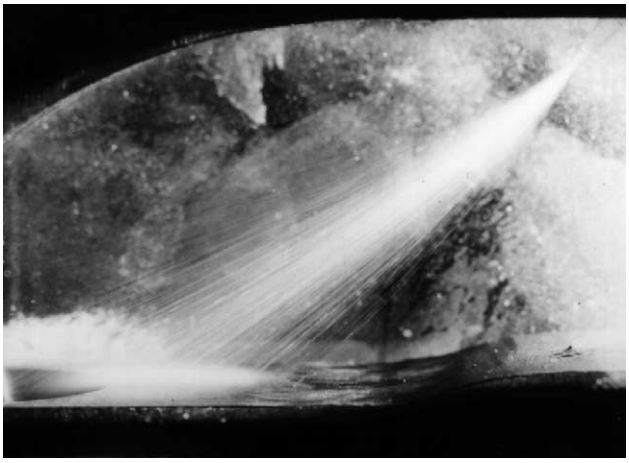

Fig. 4. Gasoline spray from injector: valve lift = 4.0 mm; $V_{\text{man. air}}$ = 18.5 m/s; injector block 1; duct depth D_H = 30 mm.

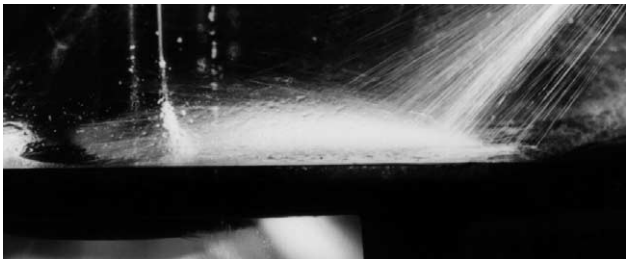

Fig. 5. Spray rebound from manifold floor: injector block 1; valve head diameter D_V = 25 mm.

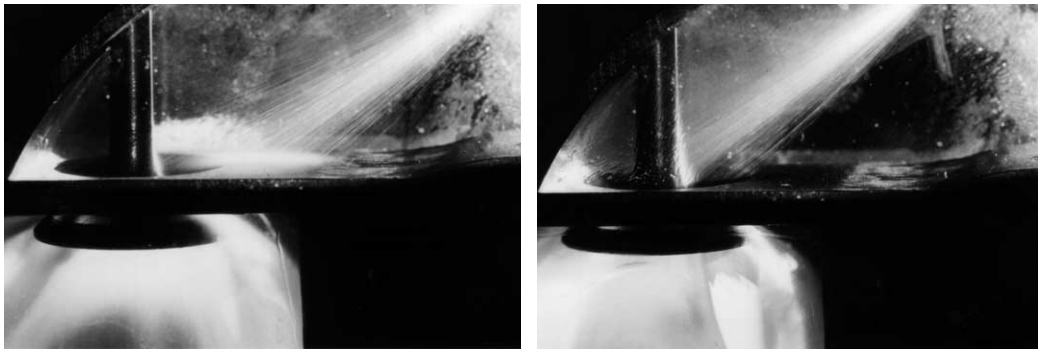

Fig. 6. Effect of injector location on port and intake valve stem fuel films: (a) block 1; (b) block 2; valve lift = 4.0 mm; $V_{\text{man. air}} = 18.5$ m/s; $V_{\text{valve air}} = 53$ m/s.

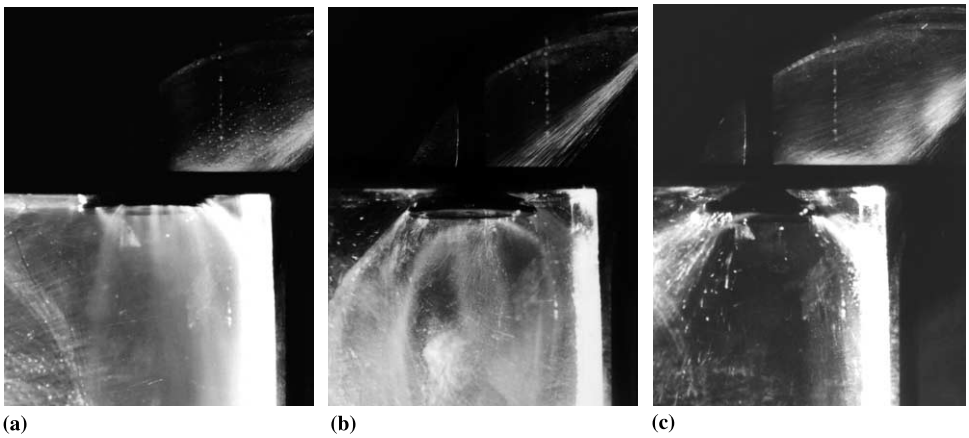

Fig. 7. Fuel flow through the inlet valve at different valve openings: (a) valve lift = 1 mm, $V_{\text{man. air}} = 10.5$ m/s, $V_{\text{valve air}} = 120$ m/s; (b) valve lift = 2.5 mm, $V_{\text{man. air}} = 17.5$ m/s, $V_{\text{valve air}} = 80$ m/s; (c) valve lift = 4 mm, $V_{\text{man. air}} = 18.5$ m/s, $V_{\text{valve air}} = 53$ m/s.

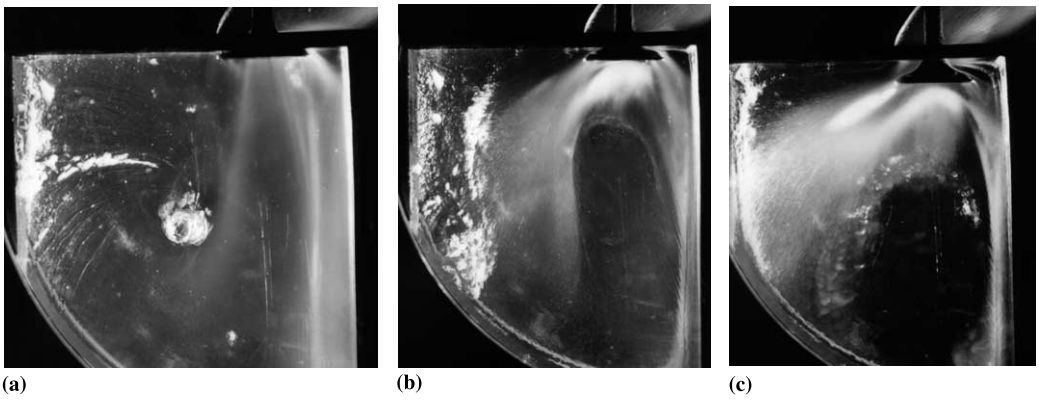

Fig. 8. Fuel distribution below the inlet valve at different valve openings: (a) valve lift = 1 mm, $V_{\text{man. air}} = 10.5$ m/s, $V_{\text{valve air}} = 120$ m/s; (b) valve lift = 2.5 mm, $V_{\text{man. air}} = 17.5$ m/s, $V_{\text{valve air}} = 80$ m/s; (c) valve lift = 4 mm, $V_{\text{man. air}} = 18.5$ m/s, $V_{\text{valve air}} = 53$ m/s.

from the upper wall from about 1 D_V (valve diameter) along it forming an extensive side wall film below that point to the far wall. The effect of the greater mass flow but slower velocity of the jet is evident at the higher valve lift.

4. Numerical simulation

The airflow through the valve has been simulated using the FLUENT code. At this stage, only the base airflow has been

considered. The droplet flow is currently being incorporated using the technique described in Milton et al. (1994). The droplet re-entrainment and re-atomisation will use models developed from the experiments reported in Milton and Behnia (1999).

Typical simulation results are shown in Figs. 9 and 10. These are taken on the centreline plane and so show some differences from the experimental views that provide an integrated picture across the full width of the test section. Also the experiments provide visualisation of the fuel flow rather than the air stream, the heavier droplets deviating from the curved air streamlines.

Nevertheless, the simulation depicts a flow that is well in accordance with the experimental results. Fig. 9 shows the velocity contours (total velocity magnitude) for the flow around the valve. At a small valve opening of 1.75 mm (Fig. 9(a)) where the manifold velocity is 10 m/s, the jet reaches a high local (maximum) velocity of around 111 m/s through the valve gap. The near side jet is directed downwards at about 60° below the horizontal and forms a clockwise vortex about 1 valve diameter (D_V) below the valve lip. On the far side, it is initially oriented about 20° downwards, becoming almost horizontal within 0.5 D_V. Regions of near 0 velocity are apparent at the vortex centre, on the lower valve face, particularly on its far side and in a triangular region below the horizontal section of the far side jet. At a larger valve opening of 4 mm (Fig. 9(b)), the manifold velocity is higher at 19 m/s but the maximum local value within the valve gap reduces to 91 m/s. The jet on both sides is now deflected some 20° further downwards towards the vertical than in the first case with near maximum velocity being maintained for almost double the distance of the previous case. The near side vortex now does not form.

The flow (again, the total velocity magnitude) below the valve in the chamber is shown in Fig. 10 for the same cases as above. At the 1.75 mm valve lift, a low velocity region exists over much of the chamber. This starts as a narrow section directly below the valve centreline and widens towards the lower, far side wall. The flow through the chamber is therefore predominantly at a high velocity down the near side wall. When the valve lift is increased to 4 mm, this low velocity region moves away from the far wall and connects to that below the far valve lip. Flow at the lower part of the chamber into the exit is now at an intermediate velocity. However, the near side velocity is still higher than that on the far side. In addition, a simulation of the flow at a valve lift of 7 mm which is higher than those used in the experiments has been carried out to examine whether this trend continues. In this case, the flow velocity is almost equal on the two sides of the chamber. However, the low velocity flow has a larger cross-sectional area and the dominant mass flow is now down the far wall. In summary, as the valve opens, the main chamber flow oscillates from the near to the far side. The reverse will occur as the valve closes.

5. Comparison of experiment and simulation

To compare the flow with experiment, velocity components in the vertical (y) direction are helpful. Using these, the motion of the flow around the valve and areas of re-circulation and separation are clearly visible as shown in Fig. 11. Note that these plots are rotated 180° from previously with the valve being on the left of the chamber. With the manifold velocity set at 15 m/s, the maximum velocity through the valve gap is 81.7 m/s, and the y-velocity components range between −54.2 and 19.4 m/s.

There are two main re-circulation zones, these being anti-clockwise below and to the left, and also clockwise to the right, of the valve. The re-circulation to the right of the valve is positioned high in the chamber compared to the experiments. However, this is a two-dimensional plot of a very complex three-dimensional flow, the figure being plotted from data at the plane of symmetry ($z = 0$). Away from the symmetry plane, both re-circulation zones become lower as can be seen by comparing Figs. 11 and 12, the latter being taken in a plane 10 mm from the centreline ($z = 10$ mm).

A comparison between the experiments and simulation is possible by examining the droplet trajectories and their distribution on the side walls. Fig. 13 is a photograph of the experimental flow with the valve in the fixed position of maximum lift (4 mm). It shows the fuel being carried through the valve gap and impinging on the neighbouring walls. With a test section depth of 30 mm and a width of 100 mm, a larger proportion of the fuel impinges on the glass walls, 15 mm from the spray centreline. Fig. 14 shows the equivalent y-velocity of the air 14 mm from the symmetry plane, that is, 1 mm from the glass wall. The fuel deposition will be predominantly in the downwash from the valve jet, the upward flow carrying little fuel. Hence, the 0 velocity contour provides a reasonable indication of the boundary of the fuel film on these walls. From Figs. 13 and 14, it can be seen that the velocities calculated from the FLUENT simulation give a distribution that compares reasonably well with the liquid spray trajectories. This 0 y-velocity contour is more clearly marked in Fig. 15 where the vertical velocity is fully shaded.

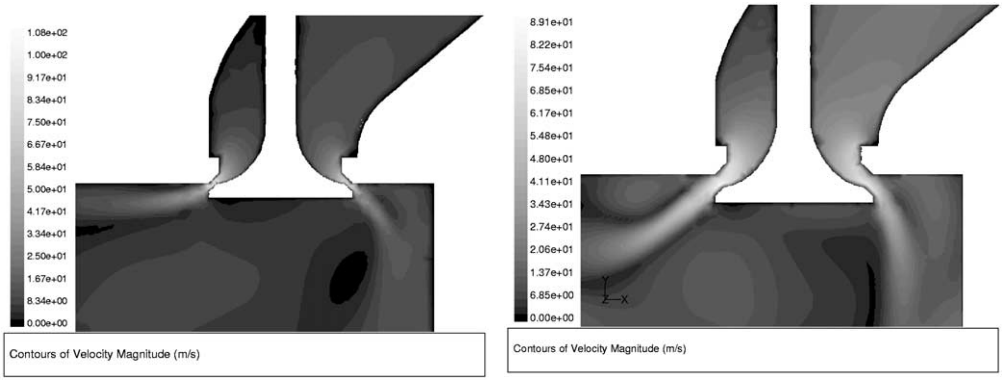

(a) (b)

Fig. 9. Air flow through the inlet valve at different valve openings: (a) valve lift = 1.75 mm, $V_{\text{man. air}} = 10.0$ m/s, $V_{\text{valve air}} = 111$ m/s (max), 65 m/s (average); (b) valve lift = 4 mm, $V_{\text{man. air}} = 18.9$ m/s, $V_{\text{valve air}} = 91$ m/s (max), 54 m/s (average).

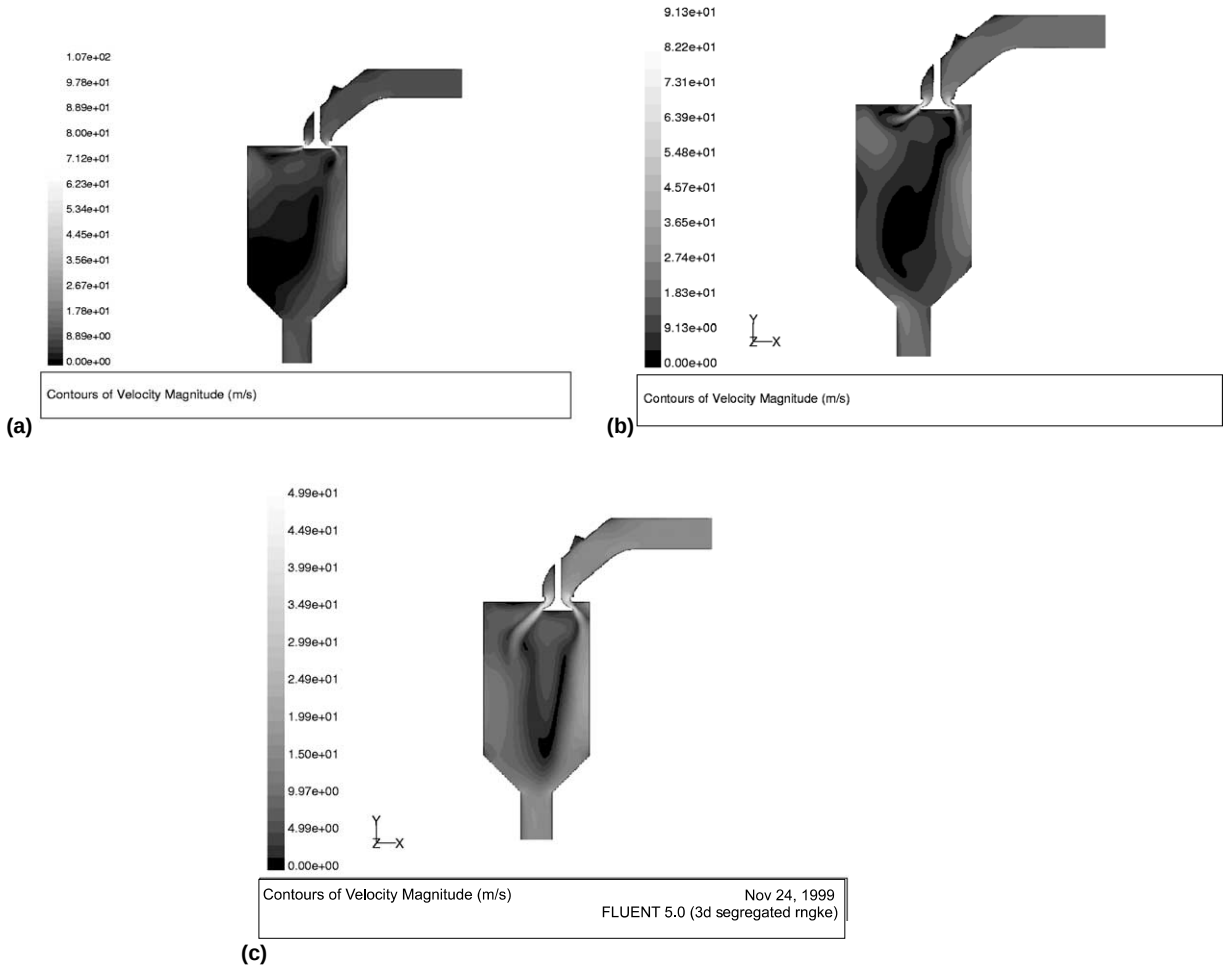

Fig. 10. Air flow within the chamber below the valve for different valve openings: (a) valve lift = 1.75 mm, $V_{\text{man. air}} = 10.0$ m/s, $V_{\text{valve air}} = 111$ m/s, (max); (b) valve lift = 4 mm, $V_{\text{man. air}} = 18.9$ m/s, $V_{\text{valve air}} = 91$ m/s, (max); (c) valve lift = 7 mm, $V_{\text{man. air}} = 21$ m/s, $V_{\text{valve air}} = 50$ m/s.

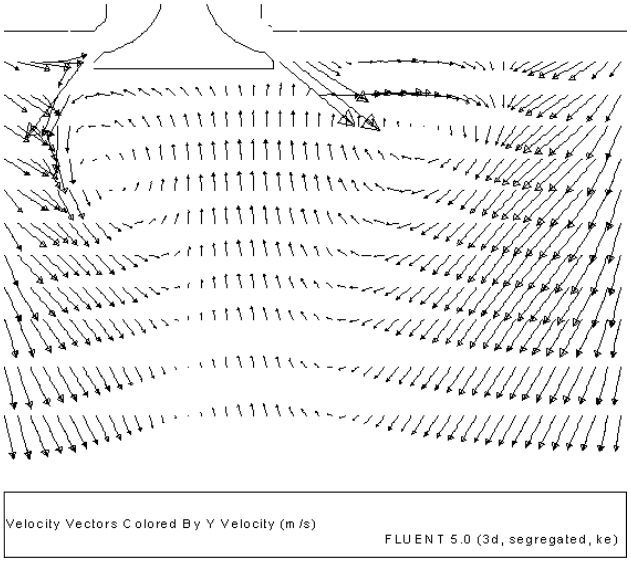

Fig. 11. Vertical (y-direction) velocity contours of air flow within the chamber in the centreline, $z = 0$ plane: valve lift = 4 mm; $V_{\text{man. air}} = 15.0$ m/s; $V_{\text{valve air}} = 81.7$ m/s (max).

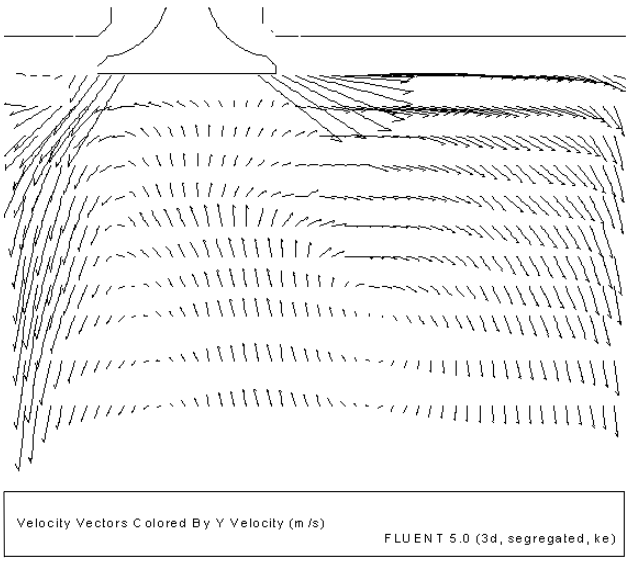

Fig. 12. Vertical (y-direction) velocity contours of air flow within the chamber in the $z = 10$ mm plane: valve lift = 4 mm; $V_{\text{man. air}} = 15.0$ m/s; $V_{\text{valve air}} = 81.7$ m/s (max).

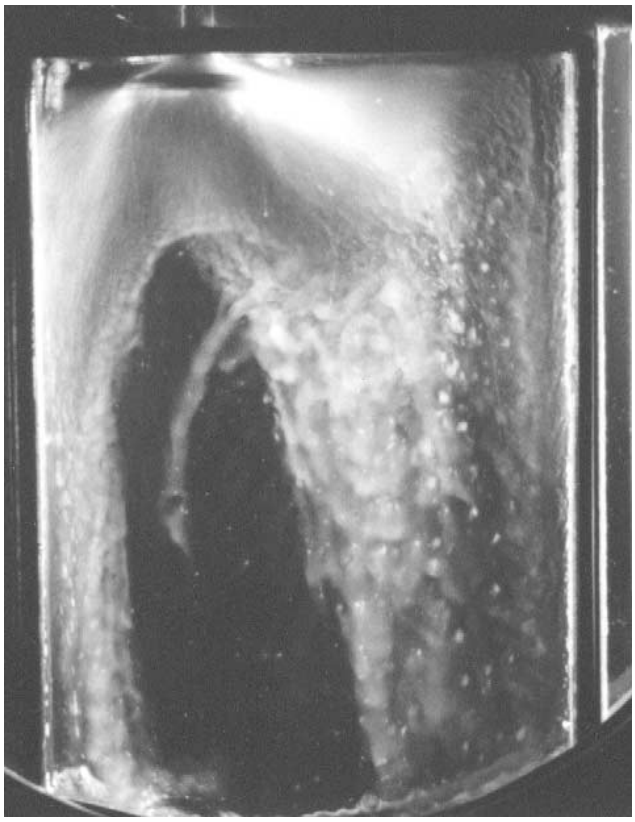

Fig. 13. Fuel distribution showing the flow patterns on the side walls ($z = 15$ mm).

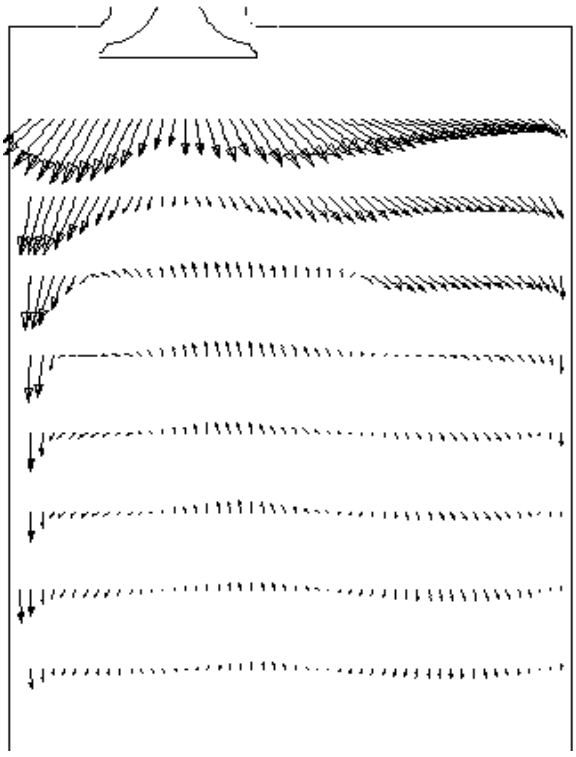

Fig. 14. y-velocity contours 1 mm from the side walls ($z = 14$ mm).

6. Conclusions

Experiments in a specially designed rig can be used with back-lit photographic techniques to show the two-phase flow through an engine-type inlet valve. The current experiments use steady flow with a series of fixed valve positions. The injector spray, fuel film formation and droplet bounce can be clearly seen. The fuel forms a film on the port floor and large droplets on the valve stem. Re-atomised fuel through the valve gap forms a heavy re-deposition onto walls in the chamber below. While some differences from a moving piston and valve and a hot chamber (as in an engine) exist, it can be inferred that there will be substantial deposition onto the engine cylinder walls in real situations, particularly under cold start

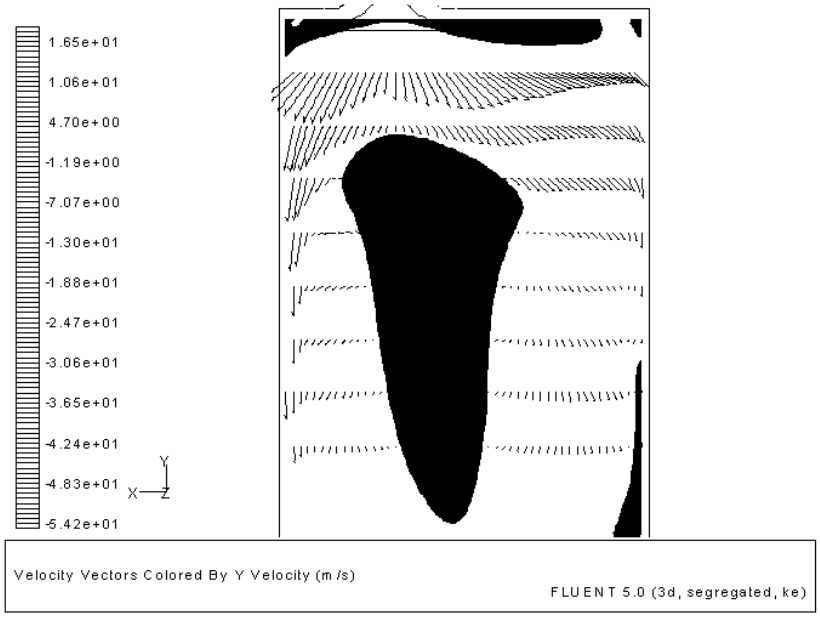

Fig. 15. Positive (downward) y-velocity components 1 mm from the side walls ($z = 14$ mm); negative y-velocities are shaded.

conditions. The importance of injector position is highlighted though it is noted that the jet deflection with different valve lifts does not allow a single, optimum location to be obtained.

Simulation of the process for the gas-phase flow using the proprietary code, FLUENT gives good agreement with experiment. A near-side vortex below the valve occurs at low valve lift (high valve throat velocity). A high velocity near side flow exists down the chamber wall. The far side jet deviates from its initial direction dictated by the valve surface towards the horizontal. A large, stagnant region exists some 4 or 5 valve diameters below the valve with the main flow oscillating from the near wall, centre to far wall as the valve lift is increased. Comparison with the experimental flow can be obtained by examining the droplet trajectories and the fuel accumulation on the side walls. The agreement is quite reasonable given that the liquid phase and its coupling with the gas-phase stream is yet to be incorporated.

The rig has been modified to include an oscillating inlet valve and experiments are underway. Further numerical studies will include coupled droplet models with the airflow in the simulation and models of stripping and re-atomisation of both the film and wall droplets in the port and on the valve stem by the high velocity gas-phase flow. Simulation of the flow with an oscillating valve will then follow.

References

Behnia, M., Milton, B.E., 1998. Two-phase fuel/air flows in spark ignition engine induction systems: experimental and numerical studies. In: Second International Symposium on Advanced Energy Conversion Systems and Related Technologies [RAN98], Nagoya, Paper 3-A-1, pp. 212–219.

Collins, M.H., 1969. A technique to characterize quantitatively the air/fuel mixture in the inlet manifold of a gasoline engine. SAE Paper 690515, Society of Automotive Engineers.

Fry, M., Nightingale, C., Richardson, S., 1995. High-speed photography and image analysis techniques applied to study droplet motion within the porting and cylinder of a 4-valve engine. SAE Paper 952525, Society of Automotive Engineers.

Hasson, D.A., Flint, W.L., 1989. An investigation of the liquid petrol wall film in the manifold of a carburetted spark ignition engine. Proc. Inst. Mech. Eng. 203 (Sect D), 77–89.

Hayashi, S., Sawa, N., 1984. A study on the transient characteristics of small SI engines. Bull. JSME 27, 224.

Hohsho, Y., Kanno, K., Nakai, H., Kadota, T., 1985. Characteristics of response of carburetted SI engine under transient conditions. Bull. JSME 28, 242.

Milton, B.E., Archer, R.D., 1998. Break-up and entrainment of liquid wall droplets by weak shock waves. In: Eighth International Symposium on Flow Visualisation, Sorrento, pp. 97.1–97.10.

Milton, B.E., Behnia, M., 1988. A numerical study of the interchanging vapour, droplet and film flows in IC engine manifolds. In: Spalding, , Afgan, (Eds.), Heat and Mass Transfer in Gasoline and Diesel Engines. Hemisphere, New York, pp. 245–258.

Milton, B.E., Behnia. M., 1999. Visualisation of fuel deposition in engine intake systems. In: Second Pacific Symposium on Flow Visualisation and Image Processing, Hawaii (CDROM).

Milton, B.E., Behnia. M., Casey, R.T., 1997. Gasoline spray and fuel deposition in the turbulent airflow field in a manifold bend or inlet port. In: Hanjalic, Peeters (Eds.), Proceedings of the Second International Symposium on Turbulence, Heat and Mass Transfer, Delft, vol. 11/12. Delft University Press, Addendum.

Milton, B.E., Behnia, M., Chen, P.Y.P., Blakeley, M.R., 1994. Simulation of fuel film formation in ducts. Int. J. Appl. Finite Elements Computer Aided Eng. 18, 349–363.

Saito, K., Sekiguchi, K., Imatake, N., Takeda, K., Yaegashi, T., 1995. A new method to analyze fuel behaviour in a spark ignition engine. SAE paper 950044, Society of Automotive Engineers.

Shayler, P.J., Teo, Y.C., Scarisbrick A., 1993. Determining fuel transfer characteristics for mixture control during transient operation. C469/008, Inst. Mech Eng., pp. 81–87.

Shin,Y., Min K., Cheng, W.K., 1995. Visualisation of mixture preparation in a port-fuel injection engine during engine warm-up. SAE paper 952481, Society of Automotive Engineers.

Takeda, K., Yaegashi, T., Sekiguchi, K., Saito, K., Imatake, N., 1995. Mixture preparation and HC emissions of a 4-valve engine with port fuel injection during cold starting and warm-up. SAE paper 950074, Society of Automotive Engineers.

Tanaka, M., Durbin, E.J., 1977. Transient response of a carburetor engine. SAE Paper 770046, Society of Automotive Engineers.

Wagner, R.M., Nemecek, L.M., Drallmeier, J.A, 1997. Fuel delivery in a port fuel injected spark ignition engine. Atomization and Sprays 7, 629–648.